Pergamon

Scripta Metallurgica *et* Materialia, Vol. 33, Nos. 10/11, pp. 1703-1708, 1995
Elsevier Science Ltd

0956-716X/95 $9.50 + .00

0956-716X(95)00411-4

MAGNETIC PROPERTIES OF CARBON-COATED Sm-Co-C AND Mn-Al-C ALLOY NANOPARTICLES

S. Kirkpatrick, M. E. McHenry, M. DeGraef, P. A. Smith,
Y. Nakamura, and D. E. Laughlin
Department of Materials Science and Engineering
Carnegie Mellon University, Pittsburgh, PA 15213-3890

E. M. Brunsman, J. H. Scott, and S. A. Majetich*
Department of Physics
Carnegie Mellon University, Pittsburgh, PA 15213-3890

(Accepted May 4,1995)

Introduction

The Huffman-Kratschmer method of preparing fullerenes has been modified for the preparation of carbon-coated nanocrystals of a variety of metals and metal carbides [1-5]. Here the graphite anode is hollowed out and packed with a mixture of metal or metal oxide powder and graphite cement. In the arc, metal-containing clusters form. The cluster stoichiometry depends on the chemistry between the metal atoms, carbon, and oxygen. The clusters diffuse until they are deposited on a surface, either the high temperature cathode or the room temperature walls of the reactor. The nanocrystalline phases produced depend on the surface temperature and the cooling rate of the clusters determined by their diffusion path and the amount of helium buffer gas [6].

This method is therefore useful in preparing metastable phases. The carbon coating common to all nanocrystals prepared by this method arises when the particles cool. Since graphite melts at a higher temperature than the metals or metal carbides we have made, phase segregation occurs in the cooling nanoparticle, forming a graphitic shell. The coating in some cases prevents degradation of air or water-sensitive compounds, a problem encountered with important magnetic materials such as $Nd_2Fe_{14}B$.

If the particles are formed from a ferromagnetic material, their size is small enough to support only a single magnetic domain. These particles are said to be superparamagnetic, and all the atomic spins align to yield a large particle moment. The particle moment rotates not through domain wall motion, but by rotating all the atomic spins together. Theories of superparamagnetism [7,8] show that the temperature dependence of the coercivity, H_c, for a uniaxial spherical particle with a single magnetic domain is given by the equation,

$$H_c = H_{ci} [1 - (T/T_B)]^{1/2}, \quad (1)$$

where H_{ci} is the coercivity at 0 K and T_B is the blocking temperature. Above the blocking temperature, the particle's magnetic moment can flip due to thermal fluctuations during the time it takes to measure the bulk

*Correspondence author.

magnetization, which for our SQUID measurements is on the order of a few minutes. Above this temperature, the particle is superparamagnetic and no hysteresis is observed in the timeframe of the measurement. Below the blocking temperature, the particle doesn't have enough thermal energy to spontaneously flip its magnetic moment in this timeframe, and nonzero coercivity is expected, with the temperature dependence given by Eq. 1. The energy, E, of the uniaxial single domain spherical magnetic particle, is

$$E = V [K \sin^2\theta + H M \cos \phi], \quad (2)$$

where V is the particle volume, K is the magnetocrystalline anisotropy, H is the applied field, and M is the particle magnetic moment. θ is the angle between the particle moment and the nearest easy axis direction, and ϕ is the angle between the applied field and the particle moment. In the absence of an applied field, the particle moment will lie along an easy axis to minimize the energy, but in a strong applied field, the moment will align with H. In order to rotate the moment to align with the field, the particle must overcome an energy barrier on the order of KV. Above the blocking temperature, the particle's magnetic moment may switch directions spontaneously due to thermal fluctuations. The blocking temperature is related to the inverse time for measuring the magnetization, ω, the attempt rate to surmount the barrier, ω_o, which is on the order of the precession frequency of the moment [8], and the height of the barrier, KV,

$$\omega = \omega_o \exp [-KV/kT_B]. \quad (3)$$

In summary, fine particle magnets may have hysteresis up to a critical temperature, just like their bulk counterparts. However, the physics responsible for the hysteretic behavior is quite different. For monodomain particles, the comparison between the thermal energy and the anisotropy energy is important, while for bulk ferromagnets the comparison between the thermal energy and the exchange energy determines the magnetic behavior.

The blocking temperature may be increased by increasing either the particle volume or the anisotropy. In the remainder of this paper we focus on alloys with large magnetocrystalline anisotropy and study the effect on the magnetic properties of alloy nanocrystals prepared in a carbon arc.

$SmCo_x$[C] Nanocrystals

Samarium cobalt has multiple stable ferromagnetic phases [9], and the magnetocrystalline anisotropy constant, K_{u1}, for $SmCo_5$ is quite large (1100×10^5 J /m^3) [10]. In preparing alloy nanocrystals of samarium cobalt in the carbon arc, we packed a mixture of graphite cement and metallic Sm_2Co_7 powder into hollowed out graphite rods. The composite rods contained approximately 6 weight percent of Sm_2Co_7. The use of an alloy starting material, rather than a mixture of metal or metal oxide powders, is desirable in order to obtain microscopic homogeneity in the arc where the nanocrystals form. We tested the raw material to optimize production conditions, and observed strong magnetic response to a $Nd_2Fe_{14}B$ magnet in powder from all parts of the reactor. Because we have observed that different phases may predominate in material from different parts of the reactor [6], due to differences in the cooling rate and the deposition temperature, we examined samples from the reactor walls and the pancake region [6] of the cathode deposit separately. In our reactor, larger volumes of material are obtained from the walls of the reactor, but the cathode deposit contains a higher fraction of nanocrystals. The fraction which is not nanocrystals is predominantly amorphous or graphitic carbon, along with smaller amounts of fullerenes.

Structural characterization of the cathode deposit pancake by X-ray diffraction (XRD) revealed the presence of $SmCo_5$, Sm_5Co_2, fcc Co, and graphite, but not Sm_2Co_7 or Sm_2Co_{17}, or samarium carbide or oxide phases. Energy dispersive spectroscopy (EDS) indicated that the Sm:Co ratio varied from region to region, in some cases cobalt rich and in others roughly equal amounts. Because the electron beam was large enough to excite atoms in multiple nanocrystals simultaneously, our apparatus could not be used to verify individual

phases found by XRD. The difference between this ratio and that in the starting material may be due to the relatively high vapor pressure of Sm. Transmission electron microscopy (TEM) showed that most particles were approximately spherical, with an average size on 20 nm and a size distribution typical of other nanocrystals made by this method [1].

Thermomagnetic analysis (TMA) is often helpful in identifying the ferromagnetic phases present in a mixture of materials. In general, the Curie temperature rises with the proportion of Co in samarium cobalt alloys [11]. While the cobalt Curie temperature was above our detection range, we expected that Sm_2Co_7 (T_c = 420 °C) [11] and $SmCo_5$ (T_c = 710 °C) [11] would be observable, even with small increases due to the addition of carbon. However, TMA showed no transitions between 25 °C and 875 °C. The addition of carbon has also been shown to increase the Curie temperature by over 260 °C in Sm_2Co_{17} cobalt magnets [11], and a similar effect may occur in $SmCo_5$. The magnetic behavior of Sm_5Co_2 is unknown, but we anticipated that it would be either paramagnetic or ferromagnetic with a very low Curie temperature.

Magnetization measurements were made on powder samples immobilized in epoxy using a Quantum Design SQUID magnetometer. The temperature was varied between 5 and 350 K, and the applied field ranged from 0 to ± 5 T. A typical hysteresis loop is shown in Fig. 1. At the maximum fields obtainable with our apparatus (5 T), the magnetization was not truly saturated. M(5 T) varied from 8.6 emu/g of sample at 5 K to 4.3 emu/g at 350 K. Since the sample is predominantly carbon, these values do not reflect the maximum obtainable figures for nanocrystals prepared by this method.

Fitting the temperature dependence of the coercivity to Eq. 1 (Fig. 2) yielded a blocking temperature of ~3800 K, far in excess of the Curie temperature for any samarium cobalt alloy. Contributions from several phases may be responsible for the deviations from linearity below 100 K. This is consistent with the presence of multiple phases detected by X-ray diffraction. As the temperature is increased above T_B for a particular component, its contribution to H_c should drop out. Since large, multidomain particles are not present in our samples, and since cobalt nanocrystals formed directly by the carbon arc process do not contribute above 150 K [1], the nonzero coercivity at 350 K must arise from samarium cobalt in some form. This hysteresis at and above room temperature is a novelty for monodomain magnetic particles.

The slope of any fit to the data in Fig. 2 cannot be interpreted in terms of a blocking temperature. The model used to understand the loss of hysteresis above the blocking temperature breaks down above T_c, where the exchange coupling between spins on neighboring atoms is disrupted by thermal fluctuations and the particle ceases to have a giant magnetic moment. Above T_c, regardless of the calculated blocking temperature, hysteresis will cease to exist.

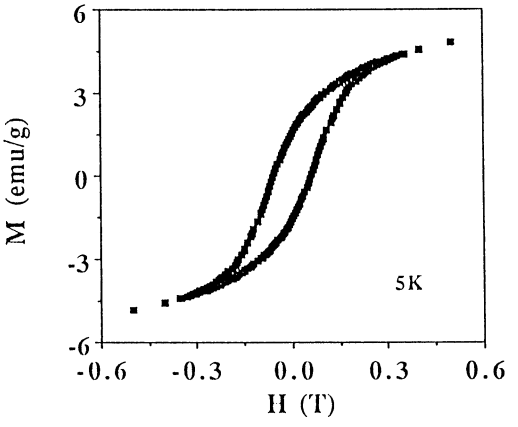

Figure 1. Magnetization as a function of the applied field for $SmCo_x$[C] sot from the pancake on the cathode deposit.

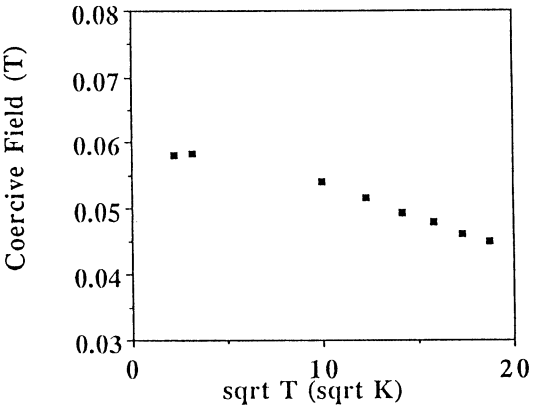

Figure 2. Coercive field as a function of $T^{1/2}$ for $SmCo_x$[C] from pancake soot.

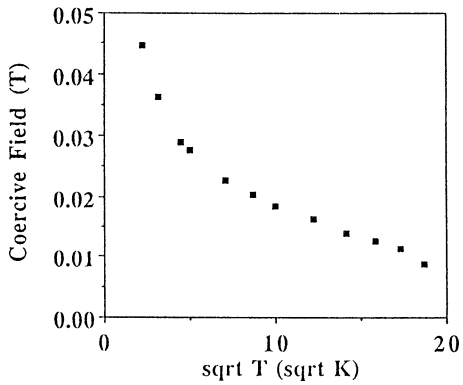

Figure 3. Coercive field as a function of $T^{1/2}$ for $SmCo_x$[C] soot from the walls of the reactor.

The magnetic behavior of a $SmCo_x$[C] sample from the walls of the copper bath reactor was also studied, and found to deviate from that of the simultaneously prepared cathode deposit. Though similarly sized nanocrystals containing both samarium and cobalt were seen by TEM with EDS, the particular phases have not yet been identified. The magnetization at 5 T drops off faster than that of the cathode deposit, from 10.0 emu/g at 3 K up 1.6 emu/g at 350 K. The low temperature deviations in the plot of the coercive field vs. $T^{1/2}$ (Fig. 3) differ from those in Fig. 2, suggesting that the presence of a phase not found in the cathode deposit. Fitting the high temperature region of Fig. 3 yields T_B = 720 K, again different from that for material formed under higher temperature conditions. Our fitting procedure determines both T_B and H_{ci}. Though the slopes of the high temperature regions in Figs. 2 and 3 look similar, the difference does not arise due to the inclusion of a measured (and multi-phase) low temperature coercivity value in the fit.

MnAl [C] Nanocrystals

In earlier preparations of elemental and carbide nanocrystals, the reactor conditions were adjusted to control the specific phases made. In order to obtain microscopic chemical homogeneity in the carbon arc, a Mn-Al-O spinel phase starting material was prepared. Stoichiometric quantities of Mn_2O_3 and Al_2O_3 were mixed, sintered at temperatures on the spinel phase field and quenched to retain the spinel phase, which was characterized by X-ray diffraction [12] and TEM analysis. The spinel phase of variable composition is identified using a Vegard's law dependence of the lattice constant on Mn:Al ratios between the two end compositions. Mn-Al-O with a 2:1 Mn:Al ratio was packed in graphite rods used in the carbon arc to generate Mn-Al-C nanoparticles.

Based on the Mn-Al-C phase diagram [13], only 1-2% carbon dissolves into the alloy, and we anticipated that the metastable phase analagous to the τ phase of MnAl would also be ferromagnetic. The only other ferromagnetic phase of Mn-Al-C was Mn_3AlC, which has a Curie temperature of 15 °C.[11] Since the τ phase is the only known ferromagnetic phase of Mn-Al-C at room temperature, raw soot from different parts of the reactor was tested with a $Nd_2Fe_{14}B$ magnet to quickly optimize the production of this ferromagnetic phase. The best arc conditions were found to be 100 A and 40 V with a 1 mm gap spacing. This lead to abundant ferromagnetic material in the pancake region [6] of the deposit which forms on the cathode. Based on a growth model for the nanocrystals made in a carbon arc, both the temperature of the surface and the cooling rate of the alloy cluster before it deposits determines the nanocrystal phase produced[6]. Here the temperature of the cathode is believed to be slightly cooler in the pancake region than in the central core deposit, but the main

factor is the difference in the cooling rate of a cluster. Bulk τ-MnAl has been made by melt cooling with a cooling rate of 10^5-10^8 °C/s, of the ε phase, followed by annealing [13].

The phases present in our sample were determined by several methods. Structural characterization by X-ray diffraction (XRD) indicated the presence of Mn_3AlC, γ-Mn, and graphite, but did not show peaks corresponding to the τ-phase. Calibration of our X-ray apparatus indicated that the *maximum* abundance of the τ phase without being able to detect it would be on the order of 4 weight percent. Energy dispersive spectroscopy (EDS) was used to determine the Mn:Al relative abundance. The ratio ranged from 3:1 to 4:1 over a wide area, consistent with the predominant species seen by XRD. We believe that at least some τ-MnAl-C is present in our samples, due to the room temperature magnetic response. Unlike in $SmCo_x$, the addition of carbon to bulk τ-MnAl reduces the Curie temperature.

High resolution TEM showed the particle shape, size, and size distribution. All particles were found to have carbon coatings, and the encapsulated nanoparticles were crystalline. An unusual feature was the presence of elongated as well as spherical particles, but the phases corresponding the the different shapes were not assigned. In the elongated particles, typical aspect ratios were on the order of three to one. If these particles are ferromagnetic, than shape anisotropy as well as magnetocrystalline anisotropy would play a role in their magnetic behavior. Both the size (average diameter ~20 nm) and the size distribution were similar to that seen in metal and metal carbide materials made by the carbon arc process [1, 6].

The magnetization as a function of the applied field and temperature was determined using SQUID magnetometry. For SQUID measurements, approximately 30 mg of platelets from the Mn-Al-C sample were immobilized, so that the nanoparticles wouldn't move in the applied magnetic field. Magnetization curves were measured between 5 and 200 K and 0 to ± 5 T. Hysteresis is observed at all temperatures within this range, and the temperature dependence of the coercive field is shown in Fig. 4. Based on the slope of this plot, hysteresis is expected up to approximately 450 K. The saturation magnetizations obtained for the Mn-Al-C samples were two orders of magnitude smaller than those for $SmCo_x$[C], suggesting that these are less promising for fine particle magnet applications.

Conclusions

The phenomenon of nonzero coercivity in monodomain ferromagnets at and above room temperature is real and has potential significance for particulate recording media. While care must be taken in the theoretical interpretation, as with elemental ferromagnet nanoparticles [14], the alloy nanoparticles enable the role of anisotropy in fine particle magnets to be explored further. Further experiments to enhance the crystallinity and

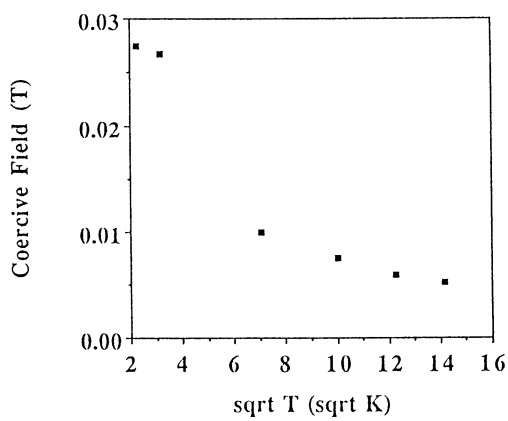

Figure 4. Coercive field as a function of $T^{1/2}$ for Mn-Al-C soot from the pancake of the cathode deposit.

therefore the magnetic properties of these materials are underway. Small ferromagnetic particles are commonly used in magnetic recording tapes, but these particles are typically much larger than those discussed in this article. Larger particle sizes have previously been used in order to obtain stability against thermal fluctuations and small changes in the applied field. Stable alloy magnet nanocrystals, such as the $SmCo_x$[C] particles prepared in a carbon arc, meet the stability requirements with smaller sizes, and are therefore a possiblity for higher density data storage medium.

Acknowledgments

S. A. M. and M. E. M. thank the NSF for support through NYI awards DMR-9258308 and DMR-9258450, respectively. The SQUID magnetometry measurements were supported in part by the NSF under grant ECD-8907068. We gratefully acknowledge the assistance of R. Obermeyer in thermomagnetic analysis measurements. Finally, support from the CMU SURG program and the assistance of members of the CMU Buckyball Project has been invaluable.

References

1. S. A. Majetich, J. O. Artman, M. E. McHenry, N. T. Nuhfer, and S. W. Staley, *Phys. Rev. B* **48**, 16845 (1993); E. M. Brunsman, M. E. McHenry, S. A. Majetich, J. O. Artman, M. De Graef, S. W. Staley, R. Sutton, E. Bortz, S. Kirkpatrick, K. Midelfort, J. Williams, and B. Brunett, *J. Appl. Phys.* **75**, 5879 (1994); M. E. McHenry, S. A. Majetich, J. O. Artman, M. DeGraef and S. W. Staley, *Phys. Rev. B* **49**, 11358 (1994); E. M. Brunsman, R. Sutton, E. Bortz, S. Kirkpatrick, K. Midelfort, J. M. Williams, P. Smith, M. E. McHenry, S. A. Majetich, J. O. Artman, and S. W. Staley, *J. Appl. Phys.* **75**, 5882 (1994).
2. M. Tomita, Y. Saito, and T. Hayashi, *Jpn. J. Appl. Phys.* **32**, L280, (1993); Y. Saito, M. Okuda, T. Yoshikawa, S. Bandow, S. Yamamuro, K. Wakoh, K. Sumiyama, and K. Suzuki, *Jpn. J. Appl. Phys.* **33**, L186 (1994); T. Hihara, H. Onodera, K. Sumiyama, K. Suzuki, A. Kasuya, Y. Nishina, Y. Saito, T. Yoshikawa, and M. Okuda, *Jpn. J. Appl. Phys.* **33**, L24 (1994).
3. R. S. Ruoff, D. C. Lorents, B. Chan, R. Malhotra, and S. Subramoney, *Science* **259**, 346, (1993).
4. S. Seraphin, D. Zhou, J. Jiao, M. A. Minke, S. Wang, T. Yadav, and J. C. Withers, *Chem. Phys. Lett.* **217**, 191 (1994); S. Seraphin, D. Zhou, J. Jiao, J. C. Withers, and R. Loutfy, *Nature* **362**, 503 (1993); S. Seraphin, D. Zhou, J. Jiao, J. C. Withers, and R. Loutfy, *Appl. Phys. Lett.* **63**, 2073 (1993).
5. Y. Yosida, *Appl. Phys. Lett.* **62**, 3447 (1993).
6. S. A. Majetich, J. H. Scott, E. M. Brunsman, M. E. McHenry, and N. T. Nuhfer, in Fullerenes: Physics, Chemistry, and New Directions VI, eds. R. S. Ruoff and K. M. Kadish, The Electrochemical Society, Pennington, NJ, 1994, p.1448; M. E. McHenry, Y. Nakamura, S. Kirkpatrick, F. Johnson, S. A. Majetich, and E. M. Brunsman, in Fullerenes: Physics, Chemistry, and New Directions VI, eds. R. S. Ruoff and K. M. Kadish, The Electrochemical Society, Pennington, NJ, 1994, p. 1463.
7. C. P. Bean and J. D. Livingston, *J. Appl. Phys.* **30**, 120S (1959).
8. I. S. Jacobs and C. P. Bean in Magnetism, Vol. 3, eds. G. T. Rado and H. Suhl, Academic Press, N.Y., 1963.
9. W. Q. Ge, C. H. Wu, and Y. C. Chuang, *Z. Metallkd.* **84**, 165 (1993).
10. D. Jiles, Introduction to Magnetism and Magnetic Materials, Chapman and Hall, London and New York, 1991, p. 124; J. M. Moreau and D. Paccard, *Acta Cryst.* **B32**, 1654 (1976).
11. K. H. Jurgen Buschow, in Materials Science and Technology, eds. Cahn, Haasen, and Kramer, 1994, pp. 451-528.
12. JCPDS-ICCD powder diffraction database.; T. Raganathan, B. E. MacKean, and A. Muan, *J. Am. Ceram. Soc.* **45**, 280 (1962).
13. A. J. McAlister and J. L. Murray, *Bull. Alloy Phase Diag.* **8**, 438 (1987); Y. J. Kim and J. H. Perepezko, *J. Appl. Phys.* **71**, 676 (1992).
14. S. Gangopadhyay, G. C. Hadjipanayis, B. Dale, C. M. Sorensen, K. J. Klabunde, V. Papaefthymiou, and A. Kostikas, *Phys. Rev. B* **45**, 9778 (1992); S. Gangopadhyay, G. C. Hadjipanayis, C. M. Sorensen, and K. J. Klabunde, *IEEE Trans. Mag.* **28**, 3174 (1992).